JOURNAL OF MATERIALS SCIENCE 21 (1986) 4024–4028

Fractographic study of the alumina and zirconia particles embedded in mullite prepared by reaction sintering

C. BAUDIN*§, F. CAMBIER‡, L. DELAEY*
*K.U.L., Department Metaalkunde en Toegepaste Materiaalkunde, Leuven, Belgium and
‡Centre de Recherches de l'Industrie de la Céramique, Mons, Belgium

Four different mullite–alumina–zirconia composites have been prepared by reaction sintering between alumina and zircon powders using magnesia or spinel ($MgAl_2O_4$) to increase the sintering and reaction rates. The microstructure of these materials can be described as composed of two parts: the first one is the mullite matrix containing various kinds of zirconia and alumina particles, whereas the second part is an amorphous phase in which alumina submatrices, zirconia and spinel particles are embedded. Examination of fracture surfaces allows one to identify the crack paths and shows that the main differences are related to zirconia inclusions. Analysis of mechanical properties and fracture features leads to the conclusion that crack deflection and microcracking are operative toughening mechanisms for the various materials. Moreover, a crack bowing mechanism is proposed to explain the higher modulus of rupture found for the series of materials prepared with magnesia as a reaction sintering aid.

1. Introduction

Mullite–alumina–zirconia composites prepared by reaction sintering (RS) of zircon–alumina mixed powders can be obtained at lower temperatures and using shorter firing times by adding small quantities of oxides such as CaO, MgO and TiO_2 [1–3]. In this case, during the process, a liquid phase appears which enhances the sintering and reaction rates. By correctly choosing the oxide quantities, this liquid phase should theoretically disappear during the heat treatment due to changes in its composition [4].

The average fracture toughness obtained for those materials is about 4 MPa $m^{1/2}$. If the classical brittle fracture equations are applied [5], large critical defects ($\approx 80\,\mu m$) are obtained from calculation. Thus, an improvement of the mechanical properties by reducing the size of the defects can be envisaged.

In the case of magnesia-containing materials, the first phase to be formed is a spinel [6] by reaction of magnesia with alumina. This reaction proceeds with a large local volume expansion impeding the process of sintering. This may be responsible for the formation of large defects; indeed, such behaviour has been observed in the sintering of TiO_2-doped mullite [7]. In order to determine the importance of this phenomenon, different materials containing on the one hand MgO + Al_2O_3, and on the other hand spinel (MgO–Al_2O_3) (as the reaction sintering aid) have been prepared. This paper describes the fracture behaviour of these two series of materials.

2. Experimental details

Mixtures of alumina, zircon and the RS aids were attrition-milled in isopropyl alcohol for one hour in relative quantities following the equation

$$2ZrSiO_4 + 0.3(MgO + Al_2O_3) + 7.4Al_2O_3 \rightarrow 2ZrO_2 + 3Al_2O_3 \cdot 2SiO_2 + 0.3MgO \cdot Al_2O_3 + 3.4Al_2O_3$$

They were then dried and isostatically pressed (200 MPa) to form parallelepipeds ($\approx$ 50 mm × 20 mm × 10 mm). Two different thermal treatments were carried out on each kind of starting mixture: firing times of 120 and 210 min for the spinel-containing samples, and 90 and 180 min for the magnesia ones (Table I). Indeed, a larger volume of lower-viscosity liquid phase can be present in the magnesia-containing samples due to possible binary SiO_2–MgO phase formation at low temperatures; this increases the RS rate when compared with the spinel-containing case.

The relative volume content of tetragonal zirconia was determined by the Garvie and Nicholson method [8] on as-fired flat surfaces.

Two mechanical properties were chosen to characterize the obtained materials: K_{Ic} and σ_F, measured on bars of about 20 mm × 3 mm × 3 mm cut from the parallelepipeds, using a three-point bending device with a span of 15 mm.

K_{Ic} determinations were performed by the single-edge notched beam ($0.2 < a/w < 0.6$) method using two different speeds ($v_1 = 0.2\,mm\,min^{-1}$, $v_2 = 0.05\,mm\,min^{-1}$) in order to determine whether subcritical crack growth could occur during its measurement. A minimum of four tests for each speed were performed, and the value of K_{Ic} calculated as the average value of

§On leave from Instituto de Ceramica Y Vidrio, CSIC, Arganda del Rey, Madrid, Spain.

0022–2461/86 $03.00 + .12

TABLE I Starting chemical composition and thermal treatments for the studied materials

Sample	Composition (wt %)				t (min)
	Al_2O_3	$ZrSiO_4$	MgO	$MgO-Al_2O_3$	
0.3 AM-120	61.38	34.60	–	4.02	120
0.3 AM-210	61.38	34.60	–	4.02	210
0.3 A + M-90	64.26	34.60	1.14	–	90
0.3 A + M-180	64.26	34.60	1.14	–	180

the measurements and the error as the standard deviation.

For modulus of rupture determinations, the sample surface in tension was softly polished with diamond (down to 2 μm) in order to avoid surface machining defects. The reported values were calculated as the average of eight experimental data, and the Weibull modulus was evaluated.

Thermal treatment at 1200° C for one hour was performed to suppress the surface tension developed during the sample machining, before conducting all the mechanical tests.

SEM micrographs were taken on gold-covered fracture surfaces of the four materials. Two kinds of fracture surface obtained in the K_{Ic} tests were studied: as-fractured twin surfaces and strongly chemically (10% HF, 1 min) and thermally (1300° C, 1 h) etched single surfaces. In order to easily distinguish the different phases, microprobe analysis results were related to secondary electrons and back-scattered electron micrographs (JEOL 733 and Cambridge 600).

To perform a quantitative analysis, the area of the particles in the fracture surface micrograph was measured on a digitizing table (Calcomp-Apple IIe) using computer facilities. The diameter of the particle area offered in the micrographs, defined as that of the equivalent circle, was corrected to obtain the real diameter by multiplying it by $4/\pi$ (taking as an approximation that the crack runs in a straight manner).

3. Results

3.1. K_{Ic} and σ_F values

Table II shows the obtained mechanical properties (K_{Ic}, σ_F). There are no differences between the K_{Ic} values measured using different loading speeds; thus subcritical crack growth seems to have been avoided. K_{Ic} values are very similar for the four tested materials.

Average σ_F and Weibull modulus values are slightly lower for the materials prepared using spinel as raw material (AM materials) and decrease with increasing firing times for both series.

3.2. Relative quantities of tetragonal zirconia

Table III shows the volume fraction of tetragonal zirconia present in the samples. A sharp decrease of this quantity occurs in the materials fired for the largest times.

TABLE II Mechanical properties

Sample	K_{Ic} (v_1) (MPa m$^{1/2}$)	K_{Ic}(v_2) (MPa m$^{1/2}$)	σ_F	Weibull modulus
0.3 AM-120	4.3 ± 0.3	4.3 ± 0.7	316 ± 33	9
0.3 AM-210	4.1 ± 0.2	4.1 ± 0.2	273 ± 26	7
0.3 A + M-90	3.8 ± 0.2	4.0 ± 0.2	341 ± 33	12
0.3 A + M-180	4.2 ± 0.2	4.0 ± 0.2	314 ± 26	10

3.3. Main fractographic features

The four studied materials can be considered as made of two parts: a mullite matrix containing various kinds of inclusion (zirconia and alumina particles) and an amorphous phase constituting discontinuities in which alumina submatrices, zirconia particles and several spinel particles are embedded. Three kinds of links are found between these two parts: hybrid zirconia particles and alumina submatrices (partly embedded in the mullite matrix and partly in the amorphous phase) and mullite–amorphous phase boundaries. The fracture behaviour of the mullite and the alumina is the same for all the studied samples, the main differences being related to the zirconia inclusions.

Figs 1 and 2 summarize the principal fractographic features observed in the four materials. In the following, fractographic features found in the mullite matrix are marked with numbers and those corresponding to the amorphous boundaries with letters.

For all the studied materials the alumina submatrices or single particles inside the mullite matrix ((1) in Fig. 1) present mainly an intergranular fracture mode, crossed alumina particles being rarely observed. Fractures run indifferently across the alumina–alumina or alumina–mullite boundaries. Three kinds of intragranular zirconia particles are found: crossed zirconia particles with no special internal structure ((2) in Fig. 1), crossed zirconia particles with internal structure ((2) and (3) in Fig 1) and non-crossed zirconia particles ((4) in Fig. 2).

Two different zirconia particle internal structures can be distinguished. The first one, present in all the samples, is found in the largest and most irregular particles and is made of different cleavage planes ((3) in Fig. 1). The second one is only found in the A + M family of materials and consists of a striped structure ((3) in Fig. 2).

Hybrid zirconia particles are found sometimes crossed ((5) in Fig. 1) and sometimes not ((6) in Fig. 1).

Flat surfaces in the amorphous phase are not found. This implies that the crack path is the boundary between this phase and the mullite matrix ((a) in Fig. 2). Nevertheless, when the other links (i.e. Al_2O_3, ZrO_2) are found the crack changes its path, sometimes crossing and at other times not crossing the zirconia particles as well as the alumina submatrices. Fig. 2 shows these features: intergranular fracture of an alumina matrix ((b) in Fig. 2), alumina submatrix surrounded by the crack ((c) in Fig. 2), crossed zirconia

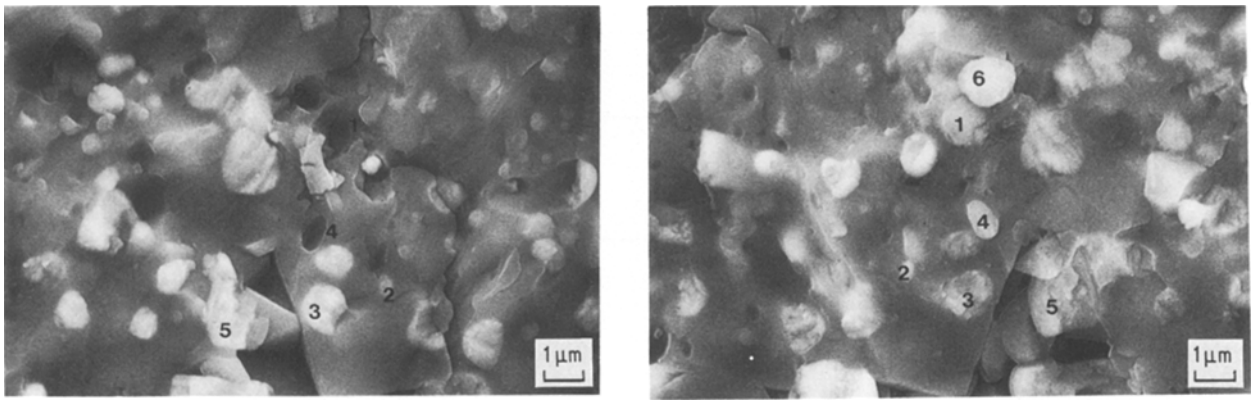

Figure 1 Pair of corresponding as-fractured surfaces (material 0.3 A + M-180). (1) Uncrossed alumina particle embedded in the mullite matrix. (2) Crossed intragranular zirconia particle showing no internal structure. (3) Crossed intragranular zirconia particle showing internal structure (different cleavage planes). (4) Uncrossed intragranular zirconia particle. (5) Crossed hybrid zirconia particle. (6) Uncrossed hybrid zirconia particle.

particles ((d) in Fig. 2) and surrounded zirconia particles ((c) in Fig. 2).

The fracture behaviour of the zirconia particles depends on their size and on the starting powders that have been used to prepare the material. For the AM family, the fracture is mainly intergranular (see Table III); only particles greater than 1.4 μm are crossed by the crack. Conversely, in the A + M materials transgranular fracture is present for particles greater than 0.4 μm.

4. Discussion

If the chemical composition alone is taken into account and assuming that the crack propagates in a straight manner [9], the expected toughness of the obtained materials is about 2.6 MPa $m^{1/2}$, which is much lower than the measured values ($\approx$4 MPa $m^{1/2}$). Such a value is however in good agreement with those previously obtained for similar materials [1–3, 9, 10].

In summary, the fracture surfaces show that the material can be considered to be made of two different parts:

Part 1. A mullite matrix inside which there are ZrO_2 and Al_2O_3 particles; this should be the "ideal material", when total homogeneity has been achieved.

Part 2. Alumina–zirconia matrix in which a glassy phase is found (a) at the triple points of the grains, and (b) in the form of bags.

There exist three kinds of links between these two parts: (a) mullite–glassy phase boundaries, (b) hybrid ZrO_2 particles and (c) hybrid Al_2O_3 particles. Different contributions to the toughening can then be considered as follows when comparing the two material parts.

4.1. Mullite matrix with inclusions (Part 1)

The most important features to be pointed out are listed below.

4.1.1. ZrO_2 inclusions

Part of the zirconia which is present in the material has been obtained in its tetragonal form. The rounded shape, smaller size and the possibility of compression forces exerted by the matrix leads us to think that it will be these particles which are retained in their tetragonal form.

Most of these particles are found to be crossed by the crack when studying the as-fractured surfaces in the A + M materials, being surrounded by it in the AM families. There exists the possibility of high zirconia in mullite solid solutions [11].

The striated substructure of some zirconia particles found in the A + M materials may come from the dendritic precipitation of ZrO_2 formed by the decomposition of the zircon in the low temperature SiO_2–MgO glass phase [12].

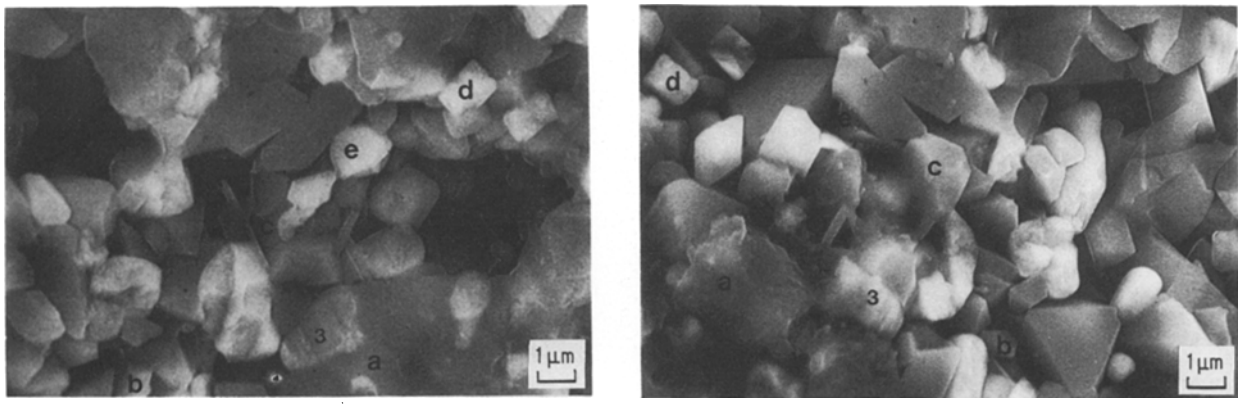

Figure 2 Pair of corresponding as-fractured surfaces (Material 0.3 A + M-180). (a) Glassy phase. (b) Alumina submatrix showing alumina–alumina intergranular fracture. (c) Fracture going across the glassy phase that surrounds the alumina submatrices. (d) Crossed intergranular zirconia particles. (e) Uncrossed intergranular zirconia particles. (3) Crossed zirconia particle showing internal structure (striated).

TABLE III Crack path of the zirconia particles in the samples fired during the longest periods

Sample	Transgranular fracture (%)	Intergranular fracture (%)	Particle size (μm)
0.3 A + M	12	88	
0.3 A + M	–	100	< 0.4
0.3 A + M	35	65	
0.3 AM	–	100	< 1
0.3 A + M	43	57	
0.3 AM	2	98	< 1.4
0.3 A + M	44	56	
0.3 AM	13	87	< 1.8

4.1.2. Al_2O_3 inclusions

Most of the particles are found to be surrounded by the crack when studying the as-fractured surfaces. The fracture behaviour seems to be the same as that of an alumina matrix of the same grain size ($< 5\,\mu$m) [13, 14].

4.1.3. Matrix

No changes in the crack path have been found due to the mullite matrix grains. The special morphology of the matrix leads to a mainly transgranular fracture mode.

4.2. Alumina–zirconia matrix with glassy phase (Part 2)

The most important facts to be considered are listed below.

4.2.1. ZrO_2 particles

Their cubic-like shape, their larger grain size and the fact that they are surrounded by a glassy phase lead us to think that they have transformed to their monoclinic form.

Most of these particles are found to be crossed by the crack when studying the as-fractured surfaces; their large size is responsible for this behaviour.

4.2.2. Al_2O_3

As for Part 1, the alumina submatrices behave as an alumina matrix of the same grain size [13, 14].

4.3. Comparison of materials

Even if the obtained K_{Ic} values are the same for the four studied materials, the different fracture behaviours observed lead us to think that different mechanisms of toughening play a role in them.

The effect of the morphology of the mullite matrix (i.e. the transgranular fracture mode through it) as well as the behaviour of the alumina submatrices is common to the four materials. Microcracks around the alumina particles can act as stress-concentrators and also produce crack branching; both phenomena increase the necessary energy for the propagation of the main crack.

Conversely, the behaviour of the zirconia particles is very different when considering one family or the other. Several facts have to be considered here. First, the K_{Ic} data are the same for materials containing 50 vol % of the total zirconia retained in its tetragonal form as for those containing only 13 vol %. Thus, the transformation toughening mechanism is not the most important one. Also, the contribution of this mechanism must be different depending on the material. In the AM family a large number of ZrO_2 particles are surrounded by the crack, and it is likely that the transformation is followed by microcracking around the particles leading to crack deflection. When the transformation is followed by microcracking the transformation work is higher [15]. Both phenomena increase the toughness of the AM materials if compared with the A + M ones.

In the A + M materials, the existence of a continuous composition change through the grain boundaries (mullite–zirconia solid solutions [11]) should lower the transformation chemical energy (i.e. the transformation work [15]) and the probability to form microcracks.

It seems then that the contribution of the zirconia particles to the material toughening is strongly related to the nature of the grain boundaries between them and the mullite matrix;

(a) In the A + M family, the strong character of the grain boundaries obliges the fracture to be transgranular; a crack-bowing phenomenon may thus be operative.

(b) In the AM family, microcracking phenomena around the zirconia particles due to their transformation in the stress field of the main crack or during cooling lead to an increase of the fracture toughness, but the flexural strengths and Weibull moduli are lowered compared with those of the A + M family.

5. Conclusions

We are dealing with four different materials which have the same chemical composition and nearly the same mechanical properties. Nevertheless, the fracture behaviour as well as the internal microstructure (i.e. grain boundaries) seem to be different. The differences are related to the zirconia particles which are placed inside the mullite grains or at the boundaries, leading to four kinds of material when considering their content (high or low) of retained tetragonal ZrO_2 and the strength (strong or weak) of the mullite–zirconia boundaries.

It seems that in terms of mechanical properties the materials behave in two different ways:

1. Macroscopically: relatively tough materials are found due to the toughening contributions of the different phases.

2. Microscopically: for the four materials, crack deflection and microcracking appear to be operative toughening mechanisms, leading however to a decrease of the flexural strength if compared with the value that could be expected. This fact is more important in the materials made using spinel as a raw material, where the ZrO_2 particles also contribute to the microcracking phenomenon.

On the other hand, a crack-bowing toughening mechanism is proposed to explain the higher σ_F values found for the series prepared using MgO as reaction sintering aid. Indeed, a transgranular fracture mode is

more commonly found through the ZrO_2 particles present in these materials.

Acknowledgement

The authors thank Professor J. S. Moya (Instituto de Ceramica Y Vidrio) for helpful discussion.

Reference

1. P. PENA, P. MIRANZO, J. S. MOYA and S. de AZA, *J. Mater. Sci.* **20** (1985) 2011.
2. P. MIRANZO, P. PENA, J. S. MOYA and S. de AZA, *ibid.* **20** (1985) 2702.
3. M. F. MELO, J. S. MOYA, P. PENA and S. de AZA, *ibid.* **20** (1985) 2711.
4. P. PENA, J. S. MOYA, S. de AZA, E. CARDINAL, F. CAMBIER, F. LEBLUD and M. R. ANSEAU, *J. Mater. Sci. Lett.* **2** (1983) 772.
5. G. K. BANSAL, *J. Amer. Ceram. Soc.* **59** (1–2) (1976) 87.
6. C. BAUDIN, CRIBC Rapport de stage (CRIBC, Mons 13, 1984).
7. C. BAUDIN and J. S. MOYA, *J. Amer. Ceram. Soc.* **67**(7) (1984) C-134.
8. R. C. GARVIE and P. S. NICHOLSON, *ibid.* **55**(6) (1972) 303.
9. C. BAUDIN, C. LEBLUD, A. LERICHE, F. CAMBIER and M. R. ANSEAU, *J. Mater. Sci. Lett.* **4** (1985) 1099.
10. G. ORANGE, G. FANTOZZI, F. CAMBIER, C. LEBLUD, M. R. ANSEAU and A. LERICHE, *J. Mater. Sci.* **20** (1985) 2533.
11. J. S. MOYA and M. I. OSENDI, *J. Mater. Sci. Lett.* **2** (1983) 599.
12. A. LERICHE, PhD thesis, University of Mons, Belgium (1986).
13. B. MUSSLER, M. V. SWAIN and N. CLAUSSEN, *J. Amer. Ceram. Soc.* **65**(11) (1982) 566.
14. G. K. BANSAL, W. H. DUCKWORTH and D. E. NIESZ, *ibid.* **59**(1–2) (1976) 472.
15. F. F. LANGE, *J. Mater. Sci.* **17** (1982) 235.

Received 6 December 1985
and accepted 24 January 1986